Journal of
Mechanics of
Materials and Structures

PROPERTY ESTIMATION IN FGM PLATES SUBJECT TO LOW-VELOCITY IMPACT LOADING

Reid A. Larson and Anthony N. Palazotto

Volume 4, Nº 7-8 September 2009

mathematical sciences publishers

JOURNAL OF MECHANICS OF MATERIALS AND STRUCTURES
Vol. 4, No. 7-8, 2009

PROPERTY ESTIMATION IN FGM PLATES SUBJECT TO LOW-VELOCITY IMPACT LOADING

REID A. LARSON AND ANTHONY N. PALAZOTTO

A property estimation sequence is presented for determining local elastic properties of a two-phased, two-constituent functionally graded material (FGM) plate subject to impact loading. The property estimation sequence combines the use of experimentally determined strain histories, finite element simulations of the experimental impact events, and an analytical model of the impact tests. The experimental, computational, and analytical models are incorporated into a parameter estimation framework, based on optimization theory, to solve for material properties of individual graded layers in the FGM plate specimens. The property estimation sequence was demonstrated using impact tests performed on a titanium-titanium boride (Ti-TiB) FGM plate system. The estimated material properties of the Ti-TiB FGM from the sequence were shown to correlate well with published material properties for the titanium-titanium boride FGM system. The estimated properties were further input into a finite element model of the impact events and were shown to approximate the experimental strain histories well. This property estimation framework is formulated to apply to virtually any two-phase FGM system and is thus an invaluable tool for research engineers studying the response of FGMs under load.

1. Introduction

Functionally graded materials (FGMs) are advanced composites with mechanical properties that vary continuously through a given dimension. The property variation, in the context of this article, is accomplished by varying the volume fraction ratio of two constituents along a given dimension. FGMs have generated a great deal of interest in recent years due to their flexibility for use in a wide variety of environments, including those structural applications where extreme thermal and corrosion resistance are required.

Most research into FGMs has occurred over the previous two decades. Suresh and Mortensen [1998] provided a comprehensive literature review of the state of the art in FGMs then prevalent, and Birman and Byrd [2007] compiled another extensive literature review covering FGM research from 1997 to 2007. Selected works pertinent to this investigation, specifically those of FGM plate statics and dynamics, will be highlighted here. J. N. Reddy and his colleagues [Reddy et al. 1999; Loy et al. 1999; Reddy 2000; Pradhan et al. 2000; Reddy and Cheng 2001; 2002] have studied the behavior of a wide variety of FGM plate configurations under static and dynamic loading, as have others in the field [Woo and Meguid 2001; Yang and Shen 2001; Yang and Shen 2002; Vel and Batra 2002; Prakash and Ganapathi 2006]. To date, only a few researchers have given consideration to studying impact response and wave propagation in functionally graded composites. Gong et al. [1999] studied low-velocity impact of FGM cylinders with various grading configurations. Bruck [2000] developed a technique to manage stress waves in discrete

Keywords: functionally graded materials, parameter estimation, impact testing.

and continuously graded FGMs in one-dimension. Li et al. [2001] first studied FGM circular plates under dynamic pressures simulating an impact load with a specific metal-ceramic system and using a rate-dependent constitutive relation they developed. Banks-Sills et al. [2002] also studied an FGM system under dynamic pressures of various temporal application. Larson et al. [2009] performed impact tests on titanium-titanium boride monolithic and functionally graded specimens and further developed finite element simulations that approximated the impact tests with a strong degree of correlation. With the exception of the last reference, all of these works were performed using analytical and computational techniques, but none of them were compared to physical or experimental data given the fact that very little test data of any kind associated with functionally graded composites can be found in the literature. This is due to (a) the difficulty to manufacture FGMs, (b) the limited availability of such materials in industry and academia, and (c) the high cost associated with producing them.

Local property estimation and accurate material models for use in FGMs present another set of unique challenges with multiphased functionally graded composites for many of the same reasons that little test data is available in the literature. To date, most investigators assume that common material models used to estimate properties in polymer-matrix fibrous composites apply in general to functionally graded materials, including those where metal and ceramic constituents are used. In this work, local elastic properties will be estimated in two-phase metal-ceramic functionally graded plates subject to impact loading using three common material models applied in a novel parameter estimation sequence. The estimation sequence combines the use of experimentally determined strain histories, finite element simulations of the experimental impact events, and an analytical model of the impact tests. The experimental, computational, and analytical models are incorporated into a parameter estimation framework, based on optimization theory, to solve for material properties of individual graded layers in the FGM plate specimens. The estimates of the local material properties can be used to study the dynamic behavior of FGM plates.

The *major contribution* of this work is a property estimation sequence that can be applied to virtually any two-phase FGM plate system under impact loading where strain data has been experimentally collected over the course of an impact event. The *key objectives* necessary to construct and validate the property estimation sequence are: (a) obtain an analytical model that reasonably approximates the conditions and results of a series of FGM plate impact tests; (b) construct a finite element model that can be used to study the FGM plate impact experiments; (c) outline the parameter estimation framework that determines FGM properties from impact data using the analytical and finite element models of the tests; and (d) correlate the FEM and experimental results using the estimated FGM properties in the finite element models for the plate specimens.

This article is organized as follows. First, an overview of FGM plate impact experiments conducted and documented in previous work by the authors is presented. Next, an analytical treatment of the impact tests is discussed based on development from previous work in the field. A finite element model of the impact tests was developed using two material models. Next, the analytical treatment and finite element model of the impact tests are used directly in a parameter estimation sequence that simultaneously determines FGM properties while matching FEM and experimental strain histories from the impact tests. Lastly, the parameter estimation sequence is demonstrated by comparing estimated material properties from an FGM system to those published in the field and comparing FEM and experimental strain histories. The article concludes with a discussion to aid future investigators in this field.

2. FGM plate impact experiments

A series of FGM plate impact tests were conducted in [Larson et al. 2009]. The results of these tests play a central role in this study, and a brief summary of the tests is presented here. The FGM system used in the tests was a titanium-titanium boride (Ti-TiB) system developed by BAE Systems – Advanced Ceramics in Vista, California. BAE Systems uses a proprietary "reaction sintering" process to produce Ti-TiB FGMs. Commercially pure titanium (Ti) and titanium diboride (TiB_2) are combined in powder form in a graphite die according to prescribed volume fractions through the plate thickness. A catalyzing agent is applied to the construction, and the powders are subjected to extreme temperature (near the melting point of titanium) and pressure in a vacuum or inert gas environment. The catalyzing agent reacts with the titanium and titanium diboride powders to form titanium boride (TiB) that crystallizes in a needle morphology. In the reaction process, almost no residual TiB_2 remains in the FGM. Through the sintering process, the powders adhere together and the Ti-TiB FGM is the final product. The change in composition of the constituents along a dimension is discrete and not truly continuous, although the distance over which a discrete change occurs can be very small and can closely approximate a continuous function over a larger distance. The FGM plates used in testing were graded over seven discrete layers of equal thickness with Ti/TiB compositions ranging from 15%/85% to 100%/0% as shown in Figure 1.

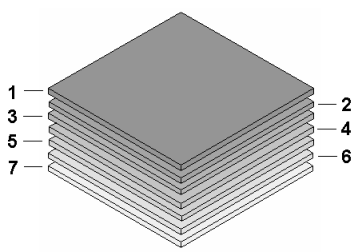

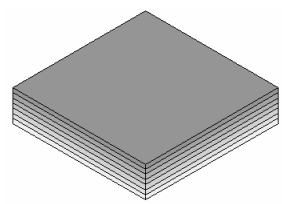

layer	% Ti	% TiB
1	15	85
2	25	75
3	40	60
4	55	45
5	70	30
6	85	15
7	100	0

Figure 1. BAE Systems Ti-TiB FGM through-the-thickness configuration of the plate specimens. The thickness of each layer is 0.181 cm.

The impact tests were conducted using the Dynatup apparatus owned by the Air Force Research Laboratory, Wright-Patterson AFB, OH. The Dynatup apparatus delivers a controlled impact load to a specimen by storing a known potential energy and converting that energy to kinetic energy prior to impact. Here, a known mass was raised above each plate specimen to a specified height and released from rest. The velocity at impact is measured by the system and can be compared to the velocity that would occur under frictionless conditions. These were the conditions for each of the four tests performed:

test	sample	crosshead/tup mass (kg)	crosshead/tup height (m)	velocity, actual (m/s)	impact energy (J)
1	7-Layer Ti-TiB FGM	13.06	0.508	3.040	60.35
2	7-Layer Ti-TiB FGM	13.06	0.635	3.412	76.02
3	7-Layer Ti-TiB FGM	13.06	0.762	3.765	92.56
4	7-Layer Ti-TiB FGM	13.06	0.889	4.078	108.6

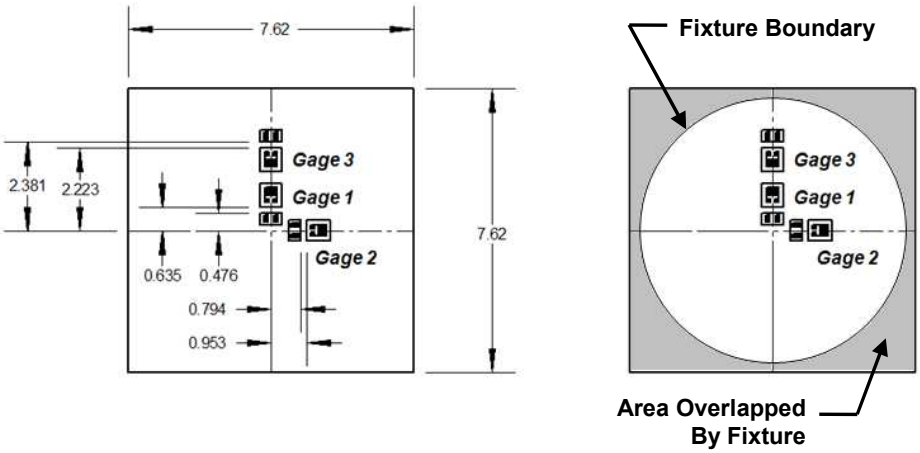

Figure 2. Specimen plate with location of three strain gages in FGM impact tests. The gages are installed on the bottom surface of the plate, opposite the surface impacted by the Dynatup. All dimensions are in centimeters.

Each of the four plates was 7.62 cm × 7.62 cm and 1.27 cm thick. The specimen plates were placed in a specially designed fixture that configured the plates so that they behaved very closely to a circular plate 6.99 cm in diameter with a *simply supported boundary condition*. Each of the four FGM specimen plates in the Dynatup were impacted on the TiB-rich surface (layer 1 in Figure 1) directly in the center of the plate with a 2.54 cm diameter tup with hemispherical tip. The opposite surface of the plate was instrumented with three strain gages as shown in Figure 2. The strain gages collected strain histories over the course of the impact events. The strain histories from each gage can be used to trace the local and global deflection of the plate using analytical and computational techniques. Strain histories from gages 2 and 3 are plotted for each of the tests in Figure 5 and will be discussed later in this article. The maximum strains from each gage and each test are shown in the table below. The FGM plate in test 4 failed midway through the test, and it is not certain whether it failed at the maximum strain level attainable had the plate not failed.

test	sample	maximum strain		
		gage 1	gage 2	gage 3
1	7-Layer Ti-TiB FGM	0.0014595	0.0013910	0.0006638
2	7-Layer Ti-TiB FGM	0.0017830	0.0014677	0.0007573
3	7-Layer Ti-TiB FGM	0.0018890	0.0017203	0.0007016
4	7-Layer Ti-TiB FGM	Failed	Failed	Failed

3. Analytical treatment of plate impacts

The first objective in constructing the property estimation sequence was to obtain an analytical model that reasonably approximates the conditions and results of the FGM plate impact tests. This section will describe the analytical model chosen for this very task. Larson [2008] demonstrated through extensive analysis of the test results that the period of impact loading in each of the FGM plate impact tests

was significantly larger than the period of the specimen plate-fixture's first natural mode. Under these conditions, the global response of the FGM plates subject to impact can be approximated by applying quasistatic analytical theory [Zukas et al. 1982; Goldsmith 1960]. Reddy et al. [1999] developed a theory for axisymmetric circular FGM plates relating classic plate theory to first-order shear deformable theory under quasistatic conditions. The mid-surface deflection of a homogeneous, axisymmetric circular plate with simply supported boundary and concentrated central load P from classical plate theory is given by (see [Ugural 1999]):

$$w_0^C(r) = \frac{P}{16\pi D}\left[2r^2 \ln\frac{r}{a} + \frac{3+\nu}{1+\nu}(a^2 - r^2)\right] \tag{3-1}$$

where r is the radial coordinate, a is the radius of the plate, and D is the flexural rigidity. The mid-surface deflection of a functionally graded plate that is first-order shear deformable is given by [Reddy et al. 1999] as

$$w_0^{\mathrm{FST}}(r) = \frac{D}{\Omega_1} w_0^C(r) + \frac{\mathcal{M}^C(r) - \mathcal{M}^C(a)}{A_{55}} + \frac{1}{4}\frac{c_2}{\Omega_1}(a^2 - r^2). \tag{3-2}$$

The radial strain at a radial coordinate r and thickness coordinate z (note $z = 0$ is the plate mid-surface) in the FGM plate can be determined from the theory of elasticity:

$$\epsilon_{rr}^{\mathrm{FST}}(r,z) = \left[z - \frac{B_{11}}{A_{11}}\right]\left\{-\frac{P}{16\pi\Omega_1}\left[4\ln\frac{r}{a} + 6 - 2\left(\frac{3+\nu}{1+\nu}\right)\right] + \frac{c_2}{2\Omega_1}\right\} + \frac{k_1}{2}. \tag{3-3}$$

The moment sum $\mathcal{M}^C$ in (3-2) is given by

$$\mathcal{M}^C = \frac{M_{rr}^C + M_{\theta\theta}^C}{1+\nu}, \tag{3-4}$$

where the radial and angular moment loads M within the plate from classical plate theory are

$$M_{rr}^C = -D_{11}\frac{d^2 w_0^C}{dr^2} - D_{12}\frac{1}{r}\frac{dw_0^C}{dr}, \quad M_{\theta\theta}^C = -D_{12}\frac{d^2 w_0^C}{dr^2} - D_{11}\frac{1}{r}\frac{dw_0^C}{dr}. \tag{3-5}$$

The constants in (3-2) and (3-3) from application of the boundary conditions are

$$c_2 = -\frac{2D}{a}\left(\frac{\nu - \Omega_2/\Omega_1 - \Omega_9}{\nu + \Omega_2/\Omega_1 + \Omega_9}\right)\frac{dw_0^C(a)}{dr}, \quad k_1 = \frac{2B_{11}}{aA_{11}}\left(-\frac{D}{\Omega_1}\frac{dw_0^C(a)}{dr} + \frac{c_2}{\Omega_1}\frac{a}{2}\right), \tag{3-6}$$

where the Ω_i are constants defined by

$$\Omega_1 = D_{11} - \frac{B_{11}^2}{A_{11}}, \quad \Omega_2 = D_{12} - \frac{B_{11}B_{12}}{A_{11}}, \quad \Omega_3 = B_{11} + B_{12}, \quad \Omega_9 = \frac{\Omega_3}{\Omega_1}\frac{B_{11}}{A_{11}} \tag{3-7}$$

in terms of material properties: A_{ij}, B_{ij}, and D_{ij}, the in-plane, bending-extension coupling, and bending stiffnesses from classic composite laminate theory (see [Daniel and Ishai 2006]); and A_{55}, the transverse shear stiffness, also from classic composite laminate theory. For brevity, the equations for the stiffnesses are not reproduced but note that the stiffnesses *are direct functions of the elastic material properties* (*elastic modulus and Poisson's ratio*) *assumed for the FGM layers*. Models for the elastic properties will be the focus of the next subsection.

The relation for strain in the FGM plates in (3-3) can be used to tie the test results to analytical theory. Knowing the radial location of the strain gages in each test from Figure 2 and the maximum strain values

for each gage in each test (see table on page 1432), the maximum contact force P can be solved for in (3-3) using known material properties. The value for the contact force P is then substituted into (3-2) to solve for the transverse deflection of the FGM plate's midsurface. This is a key aspect of estimating material properties in the FGM and will be discussed again subsequently.

A very important note on the displacement and strain of the plate is in order before proceeding. For a concentrated load, at or very near $r = 0$ the displacement and strains are unbounded. Westergaard [1926] proposed that the problem can be alleviated by using an equivalent radius r_e in place of r in these equations at the center of the plate, meaning the concentrated load is assumed to be applied over a very small area given by

$$r_e = \sqrt{1.6\, r_c^2 + h^2} - 0.675\, h, \quad r_c \le 0.5\, h. \tag{3-8}$$

Here r_c is a small radius that defines a small circular area over which the concentrated load is assumed to be distributed and h is the thickness of the plate. One can set r_c to zero for a concentrated load, if desired, in which case r_e is equal to $0.325h$. For r less than or equal to r_e, r_e is substituted for r as a constant in the equations for displacement and strain, (3-2) and (3-3) respectively. This has the effect of bounding the solutions near the plate center, although it is only an approximation to the exact solution.

3A. ***Material models.*** Material properties such as elastic modulus, Poisson's ratio, and density must be assumed for local mixtures of Ti-TiB. In the case of the seven-layer FGM, the material properties vary in discrete jumps; in a truly continuous FGM, the material properties vary in a continuous fashion as a function of the distribution of constituents. Here, three material models that estimate properties of local mixtures of constituents are presented where the "average" properties of the composite are based on functions of the volume fractions and individual properties of the constituents.

First, the classical rule-of-mixtures (ROM) directly relates the net material properties of multiphase materials to the ratio of volume fractions (V^f) of the constituents. If $\mathcal{P}$ is an arbitrary property of a two-phase mixture and $\mathcal{P}_1$ and $\mathcal{P}_2$ are arbitrary properties of the two constituents, then the relation

$$\mathcal{P} = V_1^f \mathcal{P}_1 + V_2^f \mathcal{P}_2 \tag{3-9}$$

is assumed to describe the local properties of the FGM under the classical rule-of-mixtures. Equation (3-9) is based on the Voigt model for determining longitudinal stiffnesses if both FGM phases are in a state of equal strain [Suresh and Mortensen 1998; Daniel and Ishai 2006]. The assumption that the two phases in the FGM are in a state of equal strain can be thought of as analogous to (two) springs acting in parallel to resist a longitudinal force. A force extends or compresses two springs in parallel an equal distance (i.e., equal strain) and the springs exert forces based on their appropriate spring constants (i.e., elastic moduli adjusted by volume fractions). For this reason, the Voigt model is often referred to as a "parallel" model in composite theory.

The second material model was developed by Hill [1965]. His so-called self-consistent (SC) material model was developed specifically for two-phase composite materials. The model is general enough to be assumed applicable to FGMs. Hill showed that if a series of randomly dispersed isotropic spheres served as inclusions in a homogeneous matrix and if the matrix-inclusion composite bulk material displayed statistical isotropy (that is, a significant percentage of the composite behaves isotropically and can be reasonably assumed to behave as such), then the net bulk modulus K and shear modulus G for the

composite are given by the relations

$$\frac{\delta}{K} = \frac{V_1^f}{K - K_2} + \frac{V_2^f}{K - K_1}, \quad \frac{\eta}{G} = \frac{V_1^f}{G - G_2} + \frac{V_2^f}{G - G_1} \tag{3-10}$$

where $\delta = 3 - 5\eta = K/(K + 4G/3)$, and the subscripts 1 and 2 refer to the individual phases. Equations (3-10) must be solved for K and G simultaneously. The bulk and shear moduli are related to the elastic modulus E and Poisson ratio ν by

$$K = \frac{E}{3(1-2\nu)}, \quad G = \frac{E}{2(1+\nu)}. \tag{3-11}$$

The third model was formulated by Mori and Tanaka [1973]. They demonstrated that in two-phase composites, i.e., a matrix with randomly distributed misfitting inclusions, the average internal stress in the matrix is uniform throughout the material and independent of the position of the domain where the average is obtained. They also showed that the actual stress in the matrix is the average stress in the composite plus a locally varying stress, the average of which is zero in the matrix phase. Benveniste [1987] used their analysis as the basis for developing equations that can be used to determine bulk and shear moduli for the composite material as a whole:

$$\frac{K - K_1}{K_2 - K_1} = \frac{V_2^f \Psi_1}{(1 - V_2^f) + V_2^f \Psi_1}, \quad \frac{G - G_1}{G_2 - G_1} = \frac{V_2^f \Psi_2}{(1 - V_2^f) + V_2^f \Psi_2}. \tag{3-12}$$

Ψ_1 and Ψ_2 are constants, based on the geometry of the inclusions. Berryman [1980a; 1980b] provides a formulation for inclusions with (1) spherical and (2) ellipsoid geometries. General ellipsoids can be complicated, but spherical inclusions are special cases with simple formulas for Ψ_1 and Ψ_2:

$$\Psi_1 = \frac{K_1 + (4/3)G_1}{K_2 + (4/3)G_1}, \quad \Psi_2 = \frac{G_1 + f_1}{G_2 + f_1}, \quad f_1 = \frac{G_1\,(9K_1 + 8G_1)}{6\,(K_1 + 2G_1)}. \tag{3-13}$$

Another special case of ellipsoid inclusions is that of needle-shaped inclusions; the constants Ψ_1 and Ψ_2 are given by

$$\Psi_1 = \frac{K_1 + G_1 + G_2/3}{K_2 + G_1 + G_2/3}, \quad \Psi_2 = \frac{1}{5}\left(\frac{4\,G_1}{G_1 + G_2} + 2\frac{G_1 + f_1'}{G_2 + f_1'} + \frac{K_2 + 4G_1/3}{K_2 + G_1 + G_2/3}\right), \tag{3-14}$$

with $f_1' = G_1(3K_1 + G_1)/(3K_1 + 7G_1)$. The Mori–Tanaka (MT) material model will be used for both cases of spherical (MT-S) and needle-shaped (MT-N) inclusions in this study.

Each of the three material models (rule-of-mixtures, self-consistent, and Mori–Tanaka) are important because the elastic modulus and Poisson's ratio for local mixtures of the constituents must be used to determine the A_{ij}, B_{ij}, and D_{ij} stiffnesses for the FGM plates necessary to evaluate the displacement and strains associated with the impact tests. Note that for a given set of elastic properties and set of volume fractions of the constituents in a mixture, each of the three material models will yield different properties for the mixture. This fact will be important later in the article as the property estimation sequence is applied in practice.

4. Finite element model

The second objective necessary to implement the property estimation sequence is constructing a finite element model that can be used to study the FGM plate impact experiments. A finite element model (FEM) of the plate impact tests was developed extensively [Larson et al. 2009] to study the plate impact tests in and is discussed in this section. The commercial code ABAQUS was used for this study. The model is composed of two major components: (a) the FGM specimen plate and (b) the Dynatup fixture and tup. Each of these portions has interesting features that will be briefly discussed in the following paragraphs.

4A. ***FGM plates FEM.*** Two plate finite element models were constructed to study the FGM impact tests. The first model is a two-phase representation of the FGM where elements containing only Ti or TiB properties are randomly distributed according to local volume fraction constraints in the FGM. The two-phase finite element representation of the FGM plates is shown in Figure 3. In the figure, black elements represent TiB and white elements are Ti. The material properties for commercially pure titanium [Oberg et al. 2000] are

$$\text{elastic modulus } E = 110\,\text{GPa}, \quad \text{Poisson ratio } \nu = 0.340, \quad \text{density } \rho = 4510\,\text{kg/m}^3.$$

The material properties for titanium boride [BAE 2007] are

$$\text{elastic modulus } E = 370\,\text{GPa}, \quad \text{Poisson ratio } \nu = 0.140, \quad \text{density } \rho = 4630\,\text{kg/m}^3.$$

The second model of the FGM plates is the homogenized-layers model, also shown in Figure 3. In this model, homogenized material properties are assigned to elements based on the properties of Ti and TiB and their local volume fraction ratio using one of the three material models outlined in the previous section. *The material properties in each layer of the FGM are constant.* In the figure, the layers of the FGM are shaded based on the local volume fractions of the constituents; darker layers are TiB-rich and lighter areas are Ti-rich.

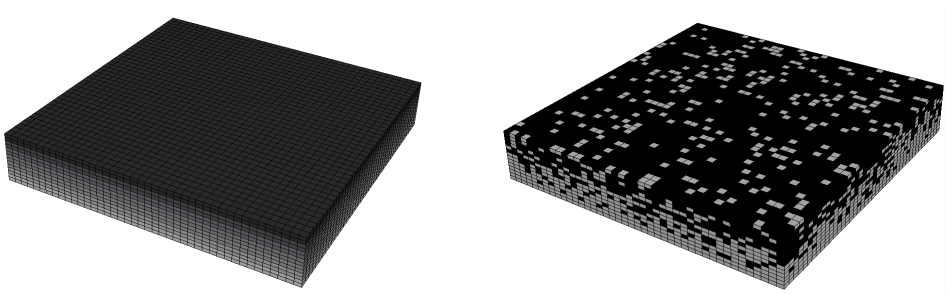

Figure 3. Schematic of specimen plate FEMs: left, homogenized-layers FEM; right, two-phase FEM.

The plates were meshed with eight-noded linear brick elements in a $42 \times 42 \times 14$-element mesh (27735 nodes and 24696 elements). The nodal grid and mesh were built using a separate mathematical script and this grid and mesh was exported to ABAQUS. The script was designed to quickly and efficiently build each grid and mesh for both the two-phase and homogenized-layers FEM of each plate.

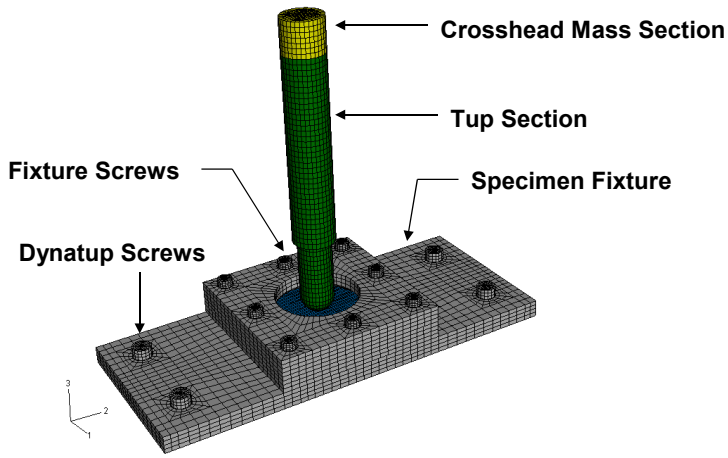

Figure 4. Finite element mesh and model for the plate impact experiments.

4B. ***Dynatup, fixture FEM.*** The second major portion of the finite element model is the Dynatup and plate fixture FEM. The plate fixture and tup FEM is shown with a specimen plate installed in Figure 4. The fixture essentially provides a boundary condition for the specimen plates very close to the actual tests (despite the fact the fixture was shown to configure the plate specimens as circular plates with simply supported boundary conditions [Larson 2008]). The specific details surrounding the plate fixture can be found in [Larson 2008; 2009]. The fixture and attachment screws were composed of 18-8 grade stainless steel and were assigned properties (1) elastic modulus, $E = 193\,\text{GPa}$; (2) Poisson ratio, $\nu = 0.290$; and (3) density, $\rho = 8030\,\text{kg/m}^3$. The same linear eight-noded brick elements as used to model the plate specimens.

The tup delivers the impact load to the plate specimens. In the FEM, the tup model stores the entire mass of the crosshead-tup assembly and a velocity field is applied to the model with the same magnitude as the impact velocity in the FGM plate tests (see table at the bottom of page 1431). The tup is meshed with eight-noded linear brick elements.

The FGM plate, fixture, and Dynatup assembly employ contact algorithms in ABAQUS to ensure the boundary conditions of the system are properly enforced. The FGM plate is in contact with the fixture components, the fixture components are in contact with each other, and the tup and FGM plate are in contact for the duration of the impact event. Additional constraints and boundary conditions were applied throughout the model as necessary to ensure the FEM reached a solution that closely emulated the conditions of the Dynatup impact tests.

5. Parameter estimation sequence

This section presents the theory and implementation of the parameter estimation sequence used to estimate FGM properties from the impact test data. This is the third objective of this work and the estimation sequence is the major contribution of this study. The section begins with an overview of general parameter estimation theory, followed by a mathematical model used to predict the plate deflection from an impact load, and then concludes with a formulated estimation sequence and its implementation.

5A. ***Overview of parameter estimation theory.*** The parameter estimation theory presented in this section is taken from standard textbooks [Arora 1989; Haftka et al. 1990; Dennis Jr. and Schnabel 1983]. The parameter estimation sequence is posed as a *constrained minimization problem*, generally defined as

$$\begin{aligned} \min \ & f(\boldsymbol{x}) = f(x_1, \ldots, x_n) \\ \text{subject to } & \boldsymbol{h}(\boldsymbol{x}) = 0 \\ \text{and } & \boldsymbol{g}(\boldsymbol{x}) \le 0. \end{aligned} \tag{5-1}$$

The *objective function* f, the *equality constraint functions* $\boldsymbol{h} = (h_1, \ldots, h_p)$ and the *inequality constraint functions* $\boldsymbol{g} = (g_1, \ldots, g_m)$ all depend on the design variable $\boldsymbol{x} = (x_1, \ldots, x_n)$. These functions can be combined into the *Lagrange function* $\mathcal{L}$, defined as

$$\mathcal{L}(\boldsymbol{x}, \boldsymbol{\lambda}, \boldsymbol{\mu}) = f(\boldsymbol{x}) + \boldsymbol{\lambda}^T \boldsymbol{h}(\boldsymbol{x}) + \boldsymbol{\mu}^T \boldsymbol{g}(\boldsymbol{x}) \tag{5-2}$$

in terms of two vectors of *Lagrange multipliers*: a vector $\boldsymbol{\lambda}$ for the p equality constraints and a vector $\boldsymbol{\mu}$ for the m inequality constraints. (The Lagrange multipliers are not functions of the design variable $\boldsymbol{x}$.)

Now recall from multivariate calculus that a *necessary* condition for a differentiable function $F(\boldsymbol{x})$ to have a local extremum (maximum or minimum) at $\boldsymbol{x}^\bullet$ is that the gradient of F be zero at $\boldsymbol{x}^\bullet$:

$$\nabla F(\boldsymbol{x}^\bullet) = \boldsymbol{0}. \tag{5-3}$$

If that condition is satisfied, a *necessary* condition for $\boldsymbol{x}^\bullet$ to be a local *minimum* of F is that the Hessian matrix

$$\boldsymbol{H} = \left[\frac{\partial^2 F}{\partial x_i \, \partial x_j} \right]_{i,j=1,\ldots,n} \tag{5-4}$$

evaluated at $\boldsymbol{x}^\bullet$ be positive semidefinite. The stronger condition that the Hessian be positive definite at $\boldsymbol{x}^\bullet$ is also *sufficient* for $\boldsymbol{x}^\bullet$ to be a local minimum. Replacing "positive" by "negative" gives conditions for maximization. An indefinite Hessian implies neither a maximum nor a minimum of F.

William Karush, in his 1939 master's thesis, gave necessary conditions for a point $\boldsymbol{x}^\bullet$ to satisfy the constrained minimization problem (5-1). These conditions, often called the Kuhn–Tucker conditions, are obtained by applying the gradient criterion (5-3) to the Lagrange function (5-2) and dualizing the inequality constraints. (In the absence of inequality constraints, of course, the problem had been solved by Lagrange.) The Kuhn–Tucker necessary conditions are

$$\begin{aligned} \frac{\partial \mathcal{L}}{\partial x_j} \equiv \frac{\partial f}{\partial x_j} + \sum_{i=1}^{p} \lambda_i^\bullet \frac{\partial h_i}{\partial x_j} + \sum_{i=1}^{m} \mu_i^\bullet \frac{\partial g_i}{\partial x_j} = 0 \quad & \text{for } j = 1, \ldots, n, \\ h_i(\boldsymbol{x}^\bullet) = 0 \quad & \text{for } i = 1, \ldots, p, \\ g_i(\boldsymbol{x}^\bullet) \le 0 \quad & \text{for } i = 1, \ldots, m, \\ \mu_i^\bullet \, g_i(\boldsymbol{x}^\bullet) = 0 \quad & \text{for } i = 1, \ldots, m, \\ \mu_i^\bullet \ge 0 \quad & \text{for } i = 1, \ldots, m. \end{aligned} \tag{5-5}$$

We will apply them directly to the FGM property estimation problem in Section 5C.

5B. ***Mathematical model for plate deflection.*** A series of simulations with the two-phase FGM plate FEM were run in order to estimate the maximum center deflection of the plate from impact by fitting a second-order polynomial to the FEM results using the method of least squares (such techniques are well documented in the literature; see for example [Myers and Montgomery 1995; Lawson and Erjavec 2001]). The second-order polynomial has the form

$$\hat{y} = b_0 + \sum_{i=1}^{k} b_i x_i + \sum_{i=1}^{k} \sum_{j=i}^{k} b_{ij} x_i x_j, \tag{5-6}$$

where $\hat{y}$ is the dependent variable being estimated, x_i $(i = 1, \ldots, k)$ are the independent variables, or "factors," of the second-order polynomial, and b_0, b_{ii}, and b_{ij} are the coefficients of the terms containing independent variables.

The math model is constructed by determining the b-coefficients. The equations for doing so can be posed in matrix and vector form by setting

$$\boldsymbol{X} = \left[\, 1 \;\; x_1 \;\; x_2 \;\; x_3 \;\; x_4 \;\; x_1^2 \;\; x_2^2 \;\; x_3^2 \;\; x_4^2 \;\; x_1x_2 \;\; x_1x_3 \;\; x_1x_4 \;\; x_2x_3 \;\; x_2x_4 \;\; x_3x_4 \,\right], \tag{5-7}$$

for a response variable with four independent variables x_i, $i = 1, \ldots, 4$. Each of the column-vector elements of $\boldsymbol{X}$ contains the values or cross-multiplied values of the independent variables for each simulation where an individual $\hat{y}$ was determined. The response variable $\hat{y}$ results of each simulation are assembled into a vector and denoted $\boldsymbol{Y}$. The response variable $\hat{y}$ in this case corresponds to the mid-surface transverse center deflection of the FGM plate from impact, w_0^{FEM}, collected in each FEM simulation. The mid-surface transverse center deflection is a function of four independent variables (discussed momentarily). The vector of coefficients $\boldsymbol{b}$ for the second-order model in (5-6) is given by

$$\boldsymbol{b} = (\boldsymbol{X}^T \boldsymbol{X})^{-1} \boldsymbol{X}^T \boldsymbol{Y}. \tag{5-8}$$

The transverse deflection of the FGM plates subject to impact is dependent on the material properties and the impact velocity of the tup (understanding that the plate geometry, configuration, and boundary condition do not change). The relevant material properties are three: elastic modulus, Poisson's ratio, and density. As discussed earlier, the FGM plates behaved elastically in impact tests at room temperature, so restricting the study to these three parameters is valid.

The material properties and behavior of the titanium constituent are well documented in the literature and are assumed to be accurate. The TiB constituent, on the other hand, is not well understood and the limited available literature shows a wide range of estimated properties [Sahay et al. 1999; Atri et al. 1999; Panda and Ravichandran 2003; 2006; Ravichandran et al. 2004]. These properties with uncertain values are variables over which to optimize. It is convenient to let the design variables be ratios rather than the property values themselves. That is, we write

$$x_1 = C_1 \equiv \frac{E_{\mathrm{TiB}}}{E_{\mathrm{Ti}}}, \quad x_2 = C_2 \equiv \frac{\nu_{\mathrm{TiB}}}{\nu_{\mathrm{Ti}}}, \quad x_3 = C_3 \equiv \frac{\rho_{\mathrm{TiB}}}{\rho_{\mathrm{Ti}}}.$$

These coefficients C_i are allowed to take values over a given range of magnitudes, corresponding to the minimum and maximum predicted values for these properties. Table 1 shows each coefficient and

variable	meaning	values: maximum (coded +1)	midrange (coded 0)	minimum (coded −1)
$x_1 = C_1$	elastic modulus coefficient	4.20	3.40	2.60
$x_2 = C_2$	Poisson's ratio coefficient	0.50	0.40	0.30
$x_3 = C_3$	density coefficient	1.10	1.00	0.90
$x_4 = v_{\text{tup}}$	tup velocity	4.128 m/s	3.493 m/s	2.858 m/s

Table 1. Factors used in Box–Behnken designed experiment.

the range of values it can assume, based on data from [Sahay et al. 1999; Atri et al. 1999; Panda and Ravichandran 2003; Ravichandran et al. 2004; Panda and Ravichandran 2006; Hill and Lin 2002]. The fourth design variable, the tup impact velocity, is also assumed to be limited to certain magnitudes based on the settings for the impact tests. These four independent variables can then be coded to range from values −1 to +1, indicating minimum value and maximum value, respectively, and a midpoint value 0.

An efficient method for generating the b-coefficients in (5-6) has been developed by Box and Behnken [1960]. The series of tests necessary to determine the b-coefficients (15 b-coefficients in all for the four factors x_i) in (5-6) are shown in Table 2. According to the Box–Behnken designed experiments, 27 tests must be conducted where $\hat{y}$ is measured (again, $\hat{y}$ is the maximum center deflection of the FGM plate denoted w_0^{FEM}) using the combination of variables and associated levels shown in Table 2. The results from the two-phase FGM plate FEM according to the prescribed simulation parameters are shown in the Table 2.

Assembling the 27×1 vector $\boldsymbol{Y}$ with the results from the tests and the 27×15 array $\boldsymbol{X}$ in (5-7) and applying the vector and array to (5-8), the b-coefficients for this set of tests is determined. The b-coefficients are then used in (5-6) and the resulting mathematical model for predicting the mid-surface transverse deflection of the FGM plate at the center ($r = 0$) is

$$\begin{aligned} w_0^{\text{FEM}} = \hat{y} = {} & -258.34 \times 10^{-6} \\ & + 22.57 \times 10^{-6} x_1 + 1.21 \times 10^{-6} x_2 + 9.25 \times 10^{-9} x_3 - 37.77 \times 10^{-6} x_4 \\ & - 3.39 \times 10^{-6} x_1^2 + 420.46 \times 10^{-9} x_2^2 - 42.04 \times 10^{-9} x_3^2 - 4.26 \times 10^{-6} x_4^2 \\ & + 142.00 \times 10^{-9} x_1 x_2 - 148.50 \times 10^{-9} x_1 x_3 + 3.60 \times 10^{-6} x_1 x_4 \\ & - 55.50 \times 10^{-9} x_2 x_3 - 90.75 \times 10^{-9} x_2 x_4 - 45.25 \times 10^{-9} x_3 x_4 \end{aligned} \tag{5-9}$$

where $-1 \le x_i \le +1$. The units of w_0^{FEM} are meters. Since the coded variables for the TiB property coefficients and tup velocity are unitless, all the b-coefficients in (5-9) are in units of meters as well.

The mathematical model was then used to predict the plate deflection at each of the 27 simulations using the coded x_i values and the results are shown in Table 2. It is easily seen that the mathematical model predicts the results from the FEM simulations very closely. This mathematical model is a key component of the parameter estimation sequence described in the following paragraphs.

The two-phase FEM was used to develop the math model (5-9) to harness effects of the random distribution of constituents. In the homogenized-layers model, localized effects from adjacent phases of materials are averaged out through the use of material models that specify constant properties for

test	coded variable				w_0^{FEM}, mm	
	x_1	x_2	x_3	x_4	result	predicted
1	−1	−1	0	0	0.2849	0.2849
2	+1	−1	0	0	0.2401	0.2401
3	−1	+1	0	0	0.2827	0.2828
4	+1	+1	0	0	0.2374	0.2374
5	0	0	−1	−1	0.2250	0.2249
6	0	0	+1	−1	0.2248	0.2248
7	0	0	−1	+1	0.3003	0.3004
8	0	0	+1	+1	0.3003	0.3004
9	0	0	0	0	0.2583	0.2583
10	−1	0	0	−1	0.2466	0.2472
11	+1	0	0	−1	0.2084	0.2093
12	−1	0	0	+1	0.3310	0.3299
13	+1	0	0	+1	0.2784	0.2776
14	0	−1	−1	0	0.2592	0.2592
15	0	+1	−1	0	0.2564	0.2567
16	0	−1	+1	0	0.2597	0.2591
17	0	+1	+1	0	0.2570	0.2568
18	0	0	0	0	0.2583	0.2583
19	0	−1	0	−1	0.2262	0.2257
20	0	+1	0	−1	0.2240	0.2231
21	0	−1	0	+1	0.3001	0.3011
22	0	+1	0	+1	0.2981	0.2988
23	−1	0	−1	0	0.2845	0.2845
24	+1	0	−1	0	0.2393	0.2391
25	−1	0	+1	0	0.2838	0.2842
26	+1	0	+1	0	0.2391	0.2393
27	0	0	0	0	0.2583	0.2583

Table 2. Box–Behnken designed experiment for four factors (see Table 1), with results from FEM (maximum transverse displacement at center of plate w_0^{FEM}) and predicted values from mathematical model.

the mixture. Thus, the transverse deflection of an FGM plate under the conditions of the impact tests discussed is much easier to predict using conventional techniques—such as through the analytical model of the FGM plate impacts discussed previously. Most FGMs tend to exhibit statistical distributions of constituents that can produce localized effects that are nearly impossible to predict without simulation tools or over-simplified assumptions. In this case, the statistical effects to the transverse deflection of the plate in a two-phase mixture are generally accounted for through the use of the least squares fit to the simulation data in (5-9).

5C. ***Material property estimation.*** The property estimation sequence is posed as the following minimization problem: minimize the error between the analytical prediction for the transverse deflection of the FGM plate mid-surface (w_0^{FST}) and the prediction for the same transverse deflection of the mid-surface predicted by the math model from the FEM simulations (w_0^{FEM}) by adjusting the material properties for the TiB constituent (adjust the vector of property coefficients $\boldsymbol{C}$) subject to bounds on the values the TiB properties can assume. Mathematically, the minimization problem from (5-1) is thus formulated as

$$\begin{aligned}
\min\ & f(\boldsymbol{C}) = \left(w_0^{\mathrm{FST}}(C_1, C_2) - w_0^{\mathrm{FEM}}(C_1, C_2, C_3)\right)^2 \\
\text{subject to}\ & g_1(\boldsymbol{C}) = C_1^{\min} - C_1 \le 0, \\
& g_2(\boldsymbol{C}) = C_1 - C_1^{\max} \le 0, \\
& g_3(\boldsymbol{C}) = C_2^{\min} - C_2 \le 0, \\
& g_4(\boldsymbol{C}) = C_2 - C_2^{\max} \le 0, \\
& g_5(\boldsymbol{C}) = C_3^{\min} - C_3 \le 0, \\
& g_6(\boldsymbol{C}) = C_3 - C_3^{\max} \le 0.
\end{aligned} \tag{5-10}$$

$f(\boldsymbol{C})$ is the objective function and the equations $g_i(\boldsymbol{C})$ in (5-10) are the *inequality* constraint equations. Essentially, by minimizing the error between w_0^{FEM} and w_0^{FST}, the error is being minimized between a model that accounts for a statistical distribution of constituents and one that homogenizes material properties in each FGM layer. This process incorporates the test data (necessary to determine w_0^{FST}), an analytical model describing w_0^{FST}, and the results of FEM simulations under the same conditions (through w_0^{FEM}). This problem can be posed for each of the FGM impact tests individually. Note that w_0^{FEM} is really a function of the TiB coefficients $\boldsymbol{C}$ and the velocity of the tup. In the w_0^{FEM} term from (5-10), the velocity of the tup at impact for an individual test is already known and is therefore a constant. Thus, only the TiB properties $\boldsymbol{C}$ need to be adjusted to evaluate w_0^{FEM}. Similarly, the velocity of the tup in the w_0^{FST} analytical term is accounted for through the strain data in the tests by solving for the maximum force applied during the impact event. The analytical model does not require the density term to evaluate w_0^{FST} because of the quasistatic assumptions. Thus, w_0^{FST} is evaluated by adjusting only the TiB coefficients associated with the elastic modulus and Poisson's ratio (C_1 and C_2). Given this information, it is therefore intuitive why w_0^{FEM} is a function of only C_1, C_2, and C_3 and w_0^{FST} is a function of only C_1, C_2 in the minimization problem (5-10).

The objective function and the constraint equations are combined into the Lagrange equation,

$$\mathcal{L} = f(\boldsymbol{C}) + \boldsymbol{\mu}^T \boldsymbol{g}(\boldsymbol{C}) \tag{5-11}$$

where $\boldsymbol{\mu}$ is the vector of Lagrange multipliers, one for each of the six inequality constraints. The minimum point of $\mathcal{L}(\boldsymbol{C})$ occurs at $[\boldsymbol{C}^\bullet, \boldsymbol{\mu}^\bullet]$, subject to the Kuhn–Tucker necessary conditions in (5-5). If the point $[\boldsymbol{C}^\bullet, \boldsymbol{\mu}^\bullet]$ is truly a minimizer of $\mathcal{L}$, then the Hessian of $\mathcal{L}$ will be at least positive semidefinite and at best positive definite to satisfy the necessary and sufficient conditions for a minimum point.

The minimization problem is solved numerically. The mathematical model (5-9) for the two-phase FEM is rather straightforward; however the analytical prediction for w_0^{FST} is very difficult to evaluate into a simple closed-form relationship because of the dependence of the stiffness terms on (potentially) complicated material models. All partial derivatives were evaluated numerically and the solution to find

the minimizer of $\mathscr{L}$ was conducted using modified Newton's method [Dennis Jr. and Schnabel 1983]. The choice of numerical solver is not unique; any appropriate numerical technique for solving for zeros to a series of equations could be used.

5D. ***Implementation.*** The following is a summary of the steps to implement the parameter estimation sequence. This sequence is demonstrated using the Ti-TiB FGM, but the steps to carry out the estimation can be used with any two-constituent material system evaluated in the manner the Ti-TiB FGM plates have been. It is assumed that a mathematical model for the finite element response of the FGM such as that in (5-9) has already been determined.

(1) Set the material properties of one constituent to be held constant, named constituent 1 here (Ti for this study). The properties of constituent 2 (TiB) will be a set of constants multiplied by the set of material properties for the first constituent:

$$\begin{aligned} &\text{FGM Constituent 1:} \quad \mathscr{P}_1, \mathscr{P}_2, \ldots, \mathscr{P}_n \\ &\text{FGM Constituent 2:} \quad C_1\mathscr{P}_1, C_2\mathscr{P}_2, \ldots, C_n\mathscr{P}_n \end{aligned}$$

(2) Determine limits for the constants as constraints on the solution.

(3) Assemble the objective function and constraints into a minimization problem (5-10). Form the Lagrange function by augmenting the objective function with the constraint relations multiplied by the set of Lagrange multipliers.

(4) Choose a set of constants $C_1, \ldots, C_n$ as an initial estimate for the properties of constituent 2 within the constraints of the set. Set the vectors of Lagrange multipliers to zero. Assemble the vector $\bar{\boldsymbol{C}}_k = [\boldsymbol{C}_k, \boldsymbol{\mu}_k]$. At this initial estimate, $k = 0$. Choose a numerical step-size (fixed or variable) appropriate for the numerical algorithm used to solve the equations.

(5) Evaluate the gradient and Hessian of $\mathscr{L}$ at $\bar{\boldsymbol{C}}_k$.

(6) Use the current properties for constituents 1 and 2 to solve for the transverse displacement of the FGM plate at the center with the mathematical model for the finite element tests, w_0^{FEM}.

(7) Using the strain gage test data (maximum radial strains) from the nominal radial plate locations and the current estimate for the material properties of constituents 1 and 2, solve for the maximum impact load P from the impact event using (3-3).

(8) The P load and the current estimate for the material properties of constituents 1 and 2 are used to solve for the maximum transverse displacement w_0^{FST} at the center of the plate using (3-2).

(9) Solve for the current estimate of $\mathscr{L}$ using the solutions of w_0^{FST}, w_0^{FEM}, and the current estimate for $\bar{\boldsymbol{C}}_k$.

(10) Perform an iteration of the numerical solver (modified Newton's method was used in this work) to solve for $\bar{\boldsymbol{C}}_{k+1}$.

(11) Evaluate the gradient and Hessian of $\mathscr{L}$ at the updated $\bar{\boldsymbol{C}}_{k+1}$.

(12) Compare the norm of $\nabla\mathscr{L}(\bar{\boldsymbol{C}}_k)$ to the norm of $\nabla\mathscr{L}(\bar{\boldsymbol{C}}_{k+1})$. If the absolute value of the difference of the two norms is less than a predefined tolerance, terminate solution and go to the next step. (Another appropriate termination criterion may be used in place of that used in this work.) Else, set $k + 1 = k$ and go to step (6).

(13) If the Hessian of $\mathscr{L}$ at the updated $\bar{\boldsymbol{C}}_{k+1}$ is positive definite and the gradient $\nabla\mathscr{L}$ at the updated $\bar{\boldsymbol{C}}_{k+1}$ is sufficiently close to zero (determined by a user-defined metric), terminate solution and analyze minimum point. If minimum point is determined to be not acceptable, adjust initial choice of $\bar{\boldsymbol{C}}_0$ and repeat process.

6. Results

The final objective of this study is to correlate the FEM and experimental results using the estimated FGM properties in the finite element models for the plate specimens. To accomplish this, the property estimation sequence must be implemented and the outputs analyzed. These tasks will be the focus of this section.

The parameter estimation sequence was conducted as described in this paper using the three material models to estimate the analytical prediction of w_0^{FST}. These models were the classic rule-of-mixtures (ROM), the self-consistent model (SC), the Mori–Tanaka estimates (needles, MT-N, and spheres, MT-S). The initial estimates for the material parameters published in this section were $C_1 = 3.40$, $C_2 = 0.40$, and $C_3 = 1.00$; essentially the center points from the Box–Behnken tests in Table 1. The choice of these initial values here was merely for conceptual convenience only and the choice of initial values is more or less arbitrary in the region of interest. The minimum and maximum constraints on the parameters are the minimum and maximum levels for each parameter shown in Table 1 relaxed by 20% in each direction. Given the high degree of correlation in the second-order math model for the two-phase FEM, it was felt that this range would be accurate to the two-phase FEM without running further simulations in the Box–Behnken FEM tests. Note that while the results published in this section may not represent global minimums of $\mathscr{L}$ (the convexity of the objective function was not evaluated because of the complex nature of the objective function) for the region of interest here, various initial estimates were taken throughout the region, including points on the boundary from the inequality constraints, and in all cases the algorithm converged to the same solution for the material parameters. The solutions found for these parameters are shown in Table 3 as tested for the three primary material models and experimental tests 1-3 (the FGM plate in Test 4 failed so data was not used in the estimation sequence from that test). When the FEM mathematical model was used to estimate w_0^{FEM} for iterations of the parameter estimation sequence, the velocity from the Dynatup experiment was used for v_{tup} and held constant. Thus, w_0^{FEM} for each estimation sequence was reduced to a function of C_1, C_2, and C_3.

The estimates for the coefficients C_1, C_2, and C_3 in Table 3 show that in general all models estimated similar results for the three parameters. The difference in results is associated directly with the material models themselves and their estimates for material properties in each layer of the FGM. To illustrate this, consider the transverse displacements at the center of the plates at the minimization of $\mathscr{L}$ summarized in Table 4. In all cases the parameter estimation sequence virtually estimated the same plate deflections at the center regardless of material model. Recall the estimation sequence was tied directly to the results of the plate experiments for all material models. Since the Ti-TiB plates should ideally have the same composition through the thickness and the plates should have the same average behavior in each layer regardless of the material model chosen, it should be expected that the parameter estimation sequence would converge to very similar material properties for each layer and adjust C_i so that the material model reflects this. In Table 6, it is evident that this is indeed the case. The material property estimates (E

test	coeff.	material model ROM	SC	MT-S	MT-N
1	C_1	2.549	2.468	2.494	2.486
	C_2	0.3478	0.3583	0.3594	0.3602
	C_3	0.9458	0.9414	0.9409	0.9408
2	C_1	2.309	2.239	2.256	2.250
	C_2	0.3468	0.3551	0.3573	0.3572
	C_3	0.9325	0.9298	0.9277	0.9281
3	C_1	2.442	2.367	2.389	2.381
	C_2	0.3355	0.3424	0.3439	0.3441
	C_3	0.9540	0.9508	0.9501	0.9501

Table 3. Comparison of predicted coefficients for TiB material properties using the parameter estimation technique and three material models. The initial estimates for the material parameters were $C_1 = 3.40,\ C_2 = 0.40,\ C_3 = 1.00$.

test	method	material model ROM	SC	MT-S	MT-N
1	plate theory, w_0^{FST}	0.25926	0.26197	0.26107	0.26136
	math model, w_0^{FEM}	0.25927	0.26198	0.26108	0.26137
2	plate theory, w_0^{FST}	0.29064	0.29336	0.29268	0.29291
	math model, w_0^{FEM}	0.29065	0.29337	0.29269	0.29292
3	plate theory, w_0^{FST}	0.30959	0.31261	0.31170	0.31199
	math model, w_0^{FEM}	0.30960	0.31262	0.31171	0.31200

Table 4. Predicted maximum center displacement of plate at center of bottom surface using the predicted TiB coefficients in Table 3. All units in millimeters.

coeff.	material model ROM	SC	MT-S	MT-N
C_1	2.433	2.358	2.380	2.372
C_2	0.3434	0.3519	0.3535	0.3538
C_3	0.9441	0.9407	0.9396	0.9397

Table 5. Comparison of predicted coefficients for TiB material properties based on an average of the results shown in Table 3.

and ν only) in each layer, based on the average results for C_i in Table 5, show a very strong degree of correlation between the layers. Further, the estimates for these layers based on C_i correlate well with the published results determined experimentally. The correlation between the published results is strongest

%Ti / %TiB	elastic modulus E, GPa					Poisson ratio ν				
	Literature	ROM	SC	MT-S	MT-N	Literature	ROM	SC	MT-S	MT-N
15 / 85	274.3	244.0	231.7	234.3	232.7	0.170	0.150	0.161	0.160	0.161
25 / 75	247.6	228.2	213.9	217.0	215.2	0.182	0.173	0.187	0.185	0.187
40 / 60	193.7	204.6	188.4	192.6	190.8	0.216	0.206	0.225	0.220	0.222
55 / 45	162.2	180.9	165.1	169.9	168.2	0.246	0.240	0.259	0.253	0.255
70 / 30	139.4	157.3	144.1	148.6	147.4	0.276	0.273	0.290	0.284	0.286
85 / 15	120.1	133.6	125.8	128.7	128.0	0.310	0.307	0.317	0.313	0.314
100 / 0	106.9	110.0	110.0	110.0	110.0	0.340	0.340	0.340	0.340	0.340

Table 6. Elastic property data from parameter estimation scheme for Ti-TiB volume ratios using the (averaged) predicted values from the four material models in the estimation sequence, compared to experimental values reported in [Hill and Lin 2002].

at low to medium volume fractions of TiB and weakest (but still pretty good) at higher volume fractions of TiB. This is likely a consequence of residual titanium diboride known to be present at higher volume fractions of TiB affecting the predictions from the estimation sequence.

The maximum impact force P in each test was related to the maximum radial strains at points on the plate. Since the force data was not collected during the tests, the strain histories from the plates were used to estimate P. The predictions of load P are affected by the material properties through the FGM plates. In Table 7, the estimated force P based on the strain histories in each test at each location are compared with the different material models used to predict C_i. The average predicted load

test	method	material model			
		ROM	SC	MT-S	MT-N
1	strain gage 1	96.24	92.57	93.61	93.22
	strain gage 2	131.75	126.82	128.16	127.61
	strain gage 3	96.35	92.88	93.73	93.32
	Average Load	**108.11**	**104.09**	**105.16**	**104.72**
2	strain gage 1	111.15	107.91	108.81	108.46
	strain gage 2	130.31	126.58	127.58	127.16
	strain gage 3	101.52	98.72	99.42	99.09
	Average Load	**114.33**	**111.07**	**111.94**	**111.57**
3	strain gage 1	121.29	117.18	118.36	117.91
	strain gage 2	157.87	152.63	154.07	153.47
	strain gage 3	97.924	94.78	95.57	95.19
	Average Load	**125.70**	**121.53**	**122.67**	**122.19**

Table 7. Predicted maximum force (kN) applied to the plate at instant of maximum center displacement using the predicted TiB coefficients in Table 3.

was calculated at each iteration of the parameter estimation sequence. The data in Table 7 yields some interesting results. First, the average P for each test matches well regardless of material model. This is another verification of the statement that the estimation sequence attempts to match the properties in each layer to the actual FGM within the framework of the material model used in the sequence. Secondly, the results show the trend that the force increases as the velocity/energy increases for each test. Lastly, the P loads individually calculated at each position vary somewhat in each test, implying variability occurred in strain gage placement on each plate.

Figure 5 show the strain histories from the homogenized-layers FEMs using the Mori–Tanaka needles (MT-N) material model results compared to the experimental strain histories for FGM plate tests 1-4 (C_i per Table 5). The other models were not plotted simply because the results were virtually the same (as demonstrated through the correlation of layer-by-layer material properties). The FEM results match the test data very well for the most part. Some of the peculiarities observed in the experimental strain histories are not captured with the optimized FEMs. These minor discrepancies can be attributed to any number of causes, including but not limited to FEM boundary conditions, strain gage-adhesive-plate interactions, and tup impacts slightly off center. The FEM determined through this process, however, correlates well with published results and was developed through a process directly tied to the physics and results of the Dynatup impact tests.

Lastly, a comment on the ability of the three material models to accurately represent the physical properties of the Ti-TiB mixtures is in order. The three material models were specifically chosen for use in the parameter estimation sequence for several important reasons. First, these models have been commonly used in the literature to analytically predict properties for a wide variety of composite materials. Second, the models are relatively easy to implement in mathematical equations and simulation computer code while simultaneously providing a reasonable estimate of property variation as the volume-fraction ratio of a two-phase mixture varies. Third, each of the models was formulated under different assumptions with respect to the geometry, configurations, and behavior of the mixtures under loading conditions. Using

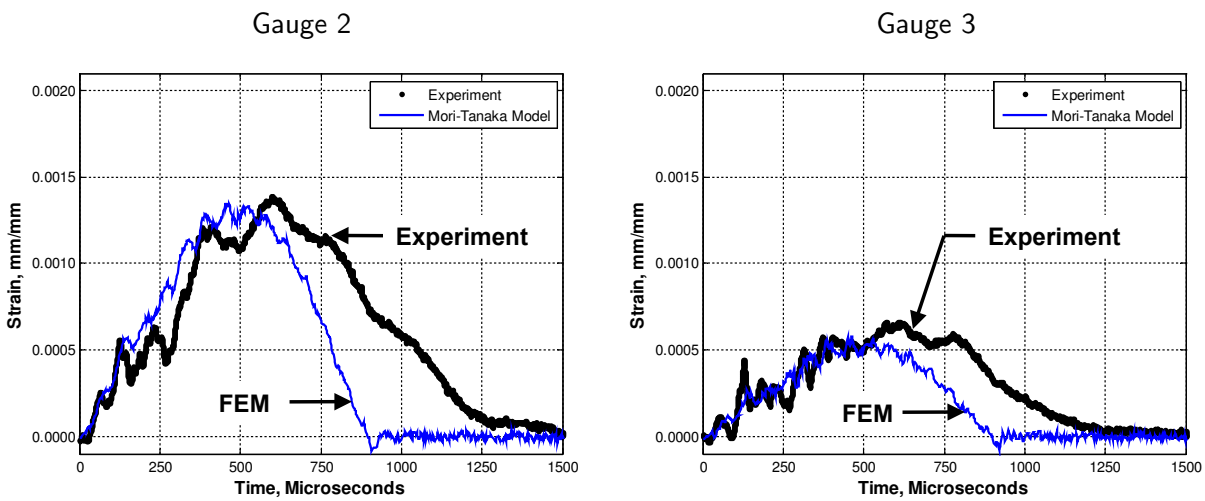

Figure 5. Experimental strain histories and FEM comparison using optimized Mori–Tanaka needles plate models, for test 1. (Continued on next page.)

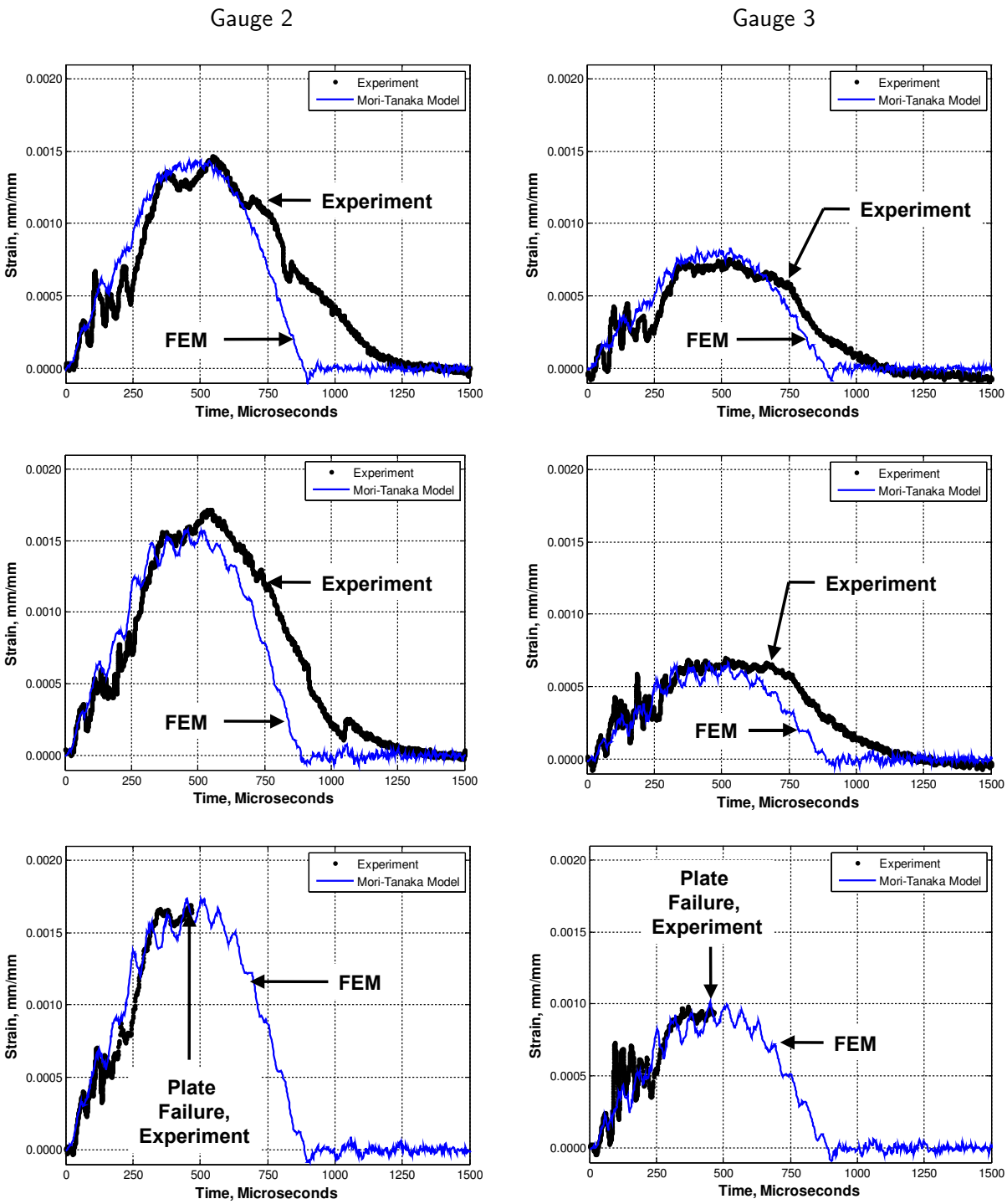

Figure 5 (continued). Experimental strain histories and FEM comparison using optimized Mori–Tanaka needles plate models, for test 2 (top), test 3 (middle) and test 4 (bottom).

each of the three models in the parameter estimation sequence then provides a means of comparison with the assumption that each of the models may be better suited to accurately predicting the physical properties of the FGM under certain conditions. The three models for the property variations and the estimates for the actual volume fraction ratios of Ti to TiB reduced the number of variables the parameter estimation sequence needed to determine. It is possible that a more robust estimation sequence could be formulated that would directly estimate material properties in individual layers of the FGMs. For example, if the sequence were to directly determine the elastic modulus, Poisson's ratio, and density of each of the seven layers of the FGM, the sequence would need to determine 21 variables (three individual properties for each of the seven layers). If such a formulation could be successfully implemented, it would likely predict physical properties more accurately than those predicted using models that may or may not accurately represent physical properties under certain conditions. However, the increased fidelity of such a formulation would come at a significant increase in computational cost.

7. Conclusions

The *major contribution* of this work is a property estimation sequence that can be applied to virtually any two-phase FGM plate system under impact loading where strain data has been experimentally collected over the course of an impact event. Each of the four *key objectives* necessary to construct and validate the property estimation sequence were realized and discussed at length: (a) obtain an analytical model that reasonably approximates the conditions and results of a series of FGM plate impact tests; (b) construct a finite element model that can be used to study the FGM plate impact experiments; (c) outline the parameter estimation framework that determines FGM properties from impact data using the analytical and finite element models of the tests; and (d) correlate the FEM and experimental results using the estimated FGM properties in the finite element models for the plate specimens. The sequence ties experimental, analytical, and computational data from FGM plate impact events together and poses the estimation sequence as a sophisticated minimization problem. The property estimation sequence was effectively demonstrated using a Ti-TiB FGM system and would be, in theory, extendable to practically any two-phased FGM system.

As a final note, the material properties determined in this study were assumed to be *rate-independent*. Given the relatively low-velocity impacts in the FGM plate tests and the fact that the plates behaved elastic to failure, the rate-independent assumption used here is likely sufficient. In high-velocity impact tests, generally rate effects become very important to the constitutive models of the system of interest. The property estimation sequence discussed here could be modified to study such problems, however the objective function and material property parameters would have to take a different form.

Acknowledgements

The views expressed in this article are those of the authors and do not reflect the official policy or position of the United States Air Force, Department of Defense, or the U.S. Government. This work was primarily funded by the Air Force Research Laboratory, Air Vehicles Directorate, Structural Science Center (AFRL/RBS); and the Dayton Area Graduate Studies Institute (DAGSI) under the AFRL/DAGSI Ohio Student-Faculty Research Fellowship Program.

References

[Arora 1989] J. S. Arora, *Introduction to optimum design*, McGraw-Hill, New York, 1989.

[Atri et al. 1999] R. R. Atri, K. S. Ravichandran, and S. K. Jha, "Elastic properties of in-situ processed Ti-TiB composites measured by impulse excitation of vibration", *Mater. Sci. Eng. A* **271**:1-2 (1999), 150–159.

[BAE 2007] Correspondence with BAE Systems sales engineer Greg Nelson, April 2007.

[Banks-Sills et al. 2002] L. Banks-Sills, R. Eliasi, and Y. Berlin, "Modeling of functionally graded materials in dynamic analyses", *Compos. B Eng.* **33**:1 (2002), 7–15.

[Benveniste 1987] Y. Benveniste, "A new approach to the application of Mori-Tanaka's theory in composite materials", *Mech. Mater.* **6**:2 (1987), 147–157.

[Berryman 1980a] J. G. Berryman, "Long-wavelength propagation in composite elastic media, I: spherical inclusions", *J. Acoust. Soc. Am.* **68**:6 (1980), 1809–1819.

[Berryman 1980b] J. G. Berryman, "Long-wavelength propagation in composite elastic media, II: ellipsoidal inclusions", *J. Acoust. Soc. Am.* **68**:6 (1980), 1820–1831.

[Birman and Byrd 2007] V. Birman and L. W. Byrd, "Modeling and analysis of functionally graded materials and structures", *Appl. Mech. Rev.* (*ASME*) **60**:5 (2007), 195–216.

[Box and Behnken 1960] G. E. P. Box and D. W. Behnken, "Some new three level designs for the study of quantitative variables", *Technometrics* **2** (1960), 455–475.

[Bruck 2000] H. A. Bruck, "A one-dimensional model for designing functionally graded materials to manage stress waves", *Int. J. Solids Struct.* **37**:44 (2000), 6383–6395.

[Daniel and Ishai 2006] I. M. Daniel and O. Ishai, *Engineering mechanics of composite materials*, 2nd ed., Oxford University Press, New York, 2006.

[Dennis Jr. and Schnabel 1983] J. E. Dennis Jr. and R. B. Schnabel, *Numerical methods for unconstrained optimization and nonlinear equations*, Prentice Hall, Englewood Cliffs, NJ, 1983.

[Goldsmith 1960] W. Goldsmith, *Impact: the theory and physical behaviour of colliding solids*, Edward Arnold, London, 1960.

[Gong et al. 1999] S. W. Gong, K. Y. Lam, and J. N. Reddy, "The elastic response of functionally graded cylindrical shells to low-velocity impact", *Int. J. Impact Eng.* **22**:4 (1999), 397–417.

[Haftka et al. 1990] R. T. Haftka, Z. Gurdal, and M. P. Kamat, *Elements of structural optimization*, 2nd ed., Kluwer, Boston, 1990.

[Hill 1965] R. Hill, "A self-consistent mechanics of composite materials", *J. Mech. Phys. Solids* **13**:4 (1965), 213–222.

[Hill and Lin 2002] M. R. Hill and W. Lin, "Residual stress measurement in a ceramic-metallic graded material", *J. Eng. Mater. Technol.* (*ASME*) **124**:2 (2002), 185–191.

[Larson 2008] R. A. Larson, "A novel method for characterizing the impact response of functionally graded plates", technical report DS/ENY/08-06, Air Force Institute of Technology, 2008, Available at http://www.stormingmedia.us/10/1096/A109684.html.

[Larson et al. 2009] R. A. Larson, A. N. Palazotto, and H. E. Gardenier, "Impact response of Ti-TiB monolithic and functionally graded composite plates", *AIAA J.* **47**:3 (March 2009), 676–691.

[Lawson and Erjavec 2001] J. Lawson and J. Erjavec, *Modern statistics for engineering and quality improvement*, Duxbury/Thomas Learning, Pacific Grove, CA, 2001.

[Li et al. 2001] Y. Li, K. T. Ramesh, and E. S. C. Chin, "Dynamic characterization of layered and graded structures under impulsive loading", *Int. J. Solids Struct.* **38**:34-35 (2001), 6045–6061.

[Loy et al. 1999] C. T. Loy, K. Y. Lam, and J. N. Reddy, "Vibration of functionally graded cylindrical shells", *Int. J. Mech. Sci.* **41**:3 (1999), 309–324.

[Mori and Tanaka 1973] T. Mori and K. Tanaka, "Average stress in matrix and average elastic energy of materials with misfitting inclusions", *Acta Metall.* **21**:5 (1973), 571–574.

[Myers and Montgomery 1995] R. H. Myers and D. C. Montgomery, *Response surface methodology: process and product optimization using designed experiments*, Wiley, New York, 1995.

[Oberg et al. 2000] E. Oberg, F. D. Jones, H. L. Horton, and H. H. Ryffel, *Machinery's handbook*, 26th ed., Industrial Press, New York, 2000.

[Panda and Ravichandran 2003] K. B. Panda and K. S. Ravichandran, "Synthesis of ductile titanium-titanium boride (Ti-TiB) composites with a beta-titanium matrix: the nature of TiB formation and composite properties", *Metall. Mater. Trans. A* **34**:6 (2003), 1371–1385.

[Panda and Ravichandran 2006] K. B. Panda and K. S. Ravichandran, "First principles determination of elastic constants and chemical bonding of titanium boride (TiB) on the basis of density functional theory", *Acta Mater.* **54**:6 (2006), 1641–1657.

[Pradhan et al. 2000] S. C. Pradhan, C. T. Loy, K. Y. Lam, and J. N. Reddy, "Vibration characteristics of functionally graded cylindrical shells under various boundary conditions", *Appl. Acoust.* **61**:1 (2000), 111–129.

[Prakash and Ganapathi 2006] T. Prakash and M. Ganapathi, "Asymmetric flexural vibration and thermoelastic stability of FGM circular plates using finite element method", *Compos. B Eng.* **37**:7-8 (2006), 642–649.

[Ravichandran et al. 2004] K. S. Ravichandran, K. B. Panda, and S. S. Sahay, "TiB_w-reinforced Ti composites: processing, properties, application prospects, and research needs", *J. Minerals Metals Mat. Soc.* **56**:5 (2004), 42–48.

[Reddy 2000] J. N. Reddy, "Analysis of functionally graded plates", *Int. J. Numer. Methods Eng.* **47**:1-3 (2000), 663–684.

[Reddy and Cheng 2001] J. N. Reddy and Z.-Q. Cheng, "Three-dimensional thermomechanical deformations of functionally graded rectangular plates", *Eur. J. Mech. A Solids* **20**:5 (2001), 841–855.

[Reddy and Cheng 2002] J. N. Reddy and Z.-Q. Cheng, "Frequency correspondence between membranes and functionally graded spherical shallow shells of polygonal planform", *Int. J. Mech. Sci.* **44**:5 (2002), 967–985.

[Reddy et al. 1999] J. N. Reddy, C. M. Wang, and S. Kitipornchai, "Axisymmetric bending of functionally graded circular and annular plates", *Eur. J. Mech. A Solids* **18**:2 (1999), 185–199.

[Sahay et al. 1999] S. S. Sahay, K. S. Ravichandran, R. Atri, B. Chen, and J. Rubin, "Evolution of microstructure and phases in situ processed Ti-TiB composites containing high volume fractions of TiB whiskers", *J. Mater. Res.* **14**:11 (1999), 4214–4223.

[Suresh and Mortensen 1998] S. Suresh and A. Mortensen, *Fundamentals of functionally graded materials: processing and thermomechanical behaviour of graded metals and metal-ceramic composites*, IOM Communications, London, 1998.

[Ugural 1999] A. C. Ugural, *Stresses in plates and shells*, 2nd ed., McGraw-Hill, Boston, 1999.

[Vel and Batra 2002] S. S. Vel and R. C. Batra, "Exact solution for thermoelastic deformations of functionally graded thick rectangular plates", *AIAA J.* **40**:7 (2002), 1421–1433.

[Westergaard 1926] H. M. Westergaard, "Stresses in concrete pavements computed by theoretical analysis", *Public Roads—U.S. Dept. of Agriculture* **7**:2 (1926), 25–35.

[Woo and Meguid 2001] J. Woo and S. A. Meguid, "Nonlinear analysis of functionally graded plates and shallow shells", *Int. J. Solids Struct.* **38**:42-43 (2001), 7409–7421.

[Yang and Shen 2001] J. Yang and H.-S. Shen, "Dynamic response of initially stressed functionally graded rectangular thin plates", *Compos. Struct.* **54**:4 (2001), 497–508.

[Yang and Shen 2002] J. Yang and H.-S. Shen, "Vibration characteristics and transient response of shear-deformable functionally graded plates in thermal environments", *J. Sound Vib.* **255**:3 (2002), 579–602.

[Zukas et al. 1982] J. A. Zukas, T. Nicholas, H. F. Swift, L. B. Greszczuk, and D. R. Curran, *Impact dynamics*, Wiley, New York, 1982.

Received 4 Dec 2008. Revised 16 Mar 2009. Accepted 13 Apr 2009.

REID A. LARSON: reid.larson@afit.edu
Air Force Institute of Technology, 2950 Hobson Way, Wright-Patterson AFB, OH 45433, United States

ANTHONY N. PALAZOTTO: anthony.palazotto@afit.edu
Air Force Institute of Technology, 2950 Hobson Way, Wright-Patterson AFB, OH 45433, United States